Available online at www.sciencedirect.com
ScienceDirect
Coordination Chemistry Reviews 252 (2008) 2480–2492
COORDINATION CHEMISTRY REVIEWS
www.elsevier.com/locate/ccr

Review

# Luminescence properties and redox behavior of Ru(II) molecular racks

Fausto Puntoriero [a], Sebastiano Campagna [a,*], Adrian-Mihail Stadler [b], Jean-Marie Lehn [b,*]

[a] *Dipartimento di Chimica Inorganica, Chimica Analitica e Chimica Fisica, Università di Messina, Via Sperone 31, 98166 Messina, Italy*
[b] *ISIS-Université Louis Pasteur, 8 Allee Gaspard Monge, BP 70028, 67083 Strasbourg cedex, France*

Received 8 October 2007; accepted 7 December 2007
Available online 20 February 2008

## Contents

1. Introduction ..... 2480
2. Molecular racks based on poly(pyridine-pyrimidine) strands ..... 2481
3. Linearly-arranged multinuclear Ru(II) complexes based on tris-terpyridine strands ..... 2483
4. Molecular racks containing naphthyridine units ..... 2484
5. Molecular grids ..... 2485
6. Ruthenium(II) molecular racks made of polytopic hydrazone-based molecular strands ..... 2487
7. Conclusions ..... 2491
Acknowledgements ..... 2491
References ..... 2491

**Abstract**

The absorption spectra, luminescence properties, and redox behavior of Ru(II) molecular racks are reviewed, together with the same properties of closely related systems, including homo- (Fe(II)) and hetero-metallic (Fe(II)/Ru(II) and Fe(II)/Os(II)) molecular grids and their mononuclear Ru(II) and Os(II) precursors, and bis-dirhodium(II, II) molecular racks. The systems discussed are based on polytopic molecular strands made of poly(pyridine-pyrimidine), poly(naphthyridine-pyrimidine), and poly(hydrazone-pyrimidine/pyrazine) subunits. Linearly-arranged systems based on tris-terpyridine molecular strands are also reported for completeness. The results indicate that the title species are quite promising multicomponent systems for the development of functional supramolecular systems, with particular regards towards the design of nano-organized species featuring information storage functions, molecular wire-type behavior, and light-harvesting antennae properties.


*Keywords:* Molecular racks; Ruthenium complexes; Supramolecular chemistry; Luminescence; Redox chemistry; Multinuclear metal complexes; Polytopic ligands

## 1. Introduction

The design and study of multinuclear metal complexes made of luminescent and redox-active subunits is an attractive research field [1,2]. Several reasons are at the basis of the interest in these species, such as the possibility to prepare organized supramolecular edifices featuring information storage functions [3] and artificial light-harvesting antennae properties [4]. Within this field, a particularly interesting class of compounds is that of the molecular racks, that is multicomponent molecular systems in which metal-based building blocks protrude from a virtually linear and rigid molecular strand [3,5]. In these species, the metal-based building blocks are "parallel" each other, and are usually orthogonal to the molecular strand alignment. Usually, molecular racks are prepared by reacting suitable metal-based moieties with multitopic molecular strands (see Fig. 1). Combination of the structural and electronic properties of the molecular strands and the "appended" metal-based moieties, along with the structural organization of the final architectures, confers specific properties to the assembly, such as particular optical, redox, and photophysical properties. It is useful to note that the molecular strands do not need to have a linear and rigid structure by themselves (for example, the multitopic strands leading to several Ru(II) racks are helical [6–8]): it is the coordination of the metal-based subunits which can impose a specific linear and

* Corresponding authors. Tel.: +39 090 6765737; fax: +39 090 393756.
*E-mail addresses:* campagna@unime.it (S. Campagna), lehn@isis.u-strasbg.fr (J.-M. Lehn).

0010-8545/$ – see front matter © 2007 Elsevier B.V. All rights reserved.
doi:10.1016/j.ccr.2007.12.009

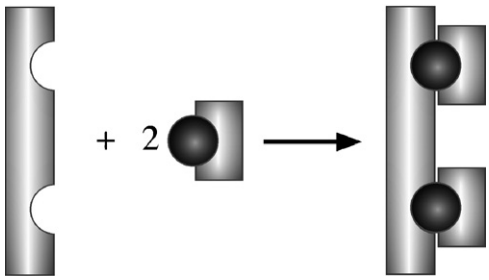

Fig. 1. Schematic representation of the synthesis of molecular racks.

rigid conformation to the assembly (in other words, the linear arrangement is "programmed" within the molecular strands, and it is "read out" by suitable metal-based components).

Here we overview the absorption spectra, excited-state (in particular, luminescence) properties, and redox behavior of some Ru(II) molecular racks we have investigated in the last 10 years, together with the properties of molecular grids containing the same or related metal-based subunits. The general schemes of synthesis of all the compounds discussed in this review are summarized in Scheme 1. More details, as well as the structures of the compounds **1**–**23** whose properties will be overviewed in this article, are given in the various chapters of the text.

## 2. Molecular racks based on poly(pyridine-pyrimidine) strands

The most known family of luminescent and redox-active ruthenium(II) complexes is that of the polypyridine complexes [1,9,10]. It was therefore straightforward to use polypyridine frameworks to design Ru(II) molecular racks. Indeed, a rack-type arrangement was obtained by using a pyrimidine ring interposed by two bipyridine moieties to generate a ditopic strand having two available terpy-like chelating sites (terpy = 2,2′:6′,2″-terpyridine) [5]. The available terpy-like chelating sites were loaded with two $Ru(terpy)^{2+}$ subunits, and the first molecular rack **1** was immediately prepared (see Chart 1). Several dinuclear racks were also prepared, having various substituents at the 5 position (the one between the two N atoms) of the pyrimidine ring [5]. Such substituents have the role to "fill the space" between the $Ru(terpy)^{2+}$ subunits in the structure, and to modify the effective structure by fine tuning the geometry of the racks, in particular the dihedral angle between the two terpy ligands. The most interesting of such species from a photochemical point of view was compound **2**, contaning an additional chromophore, the anthracene (Chart 1) [11]. The absorption spectrum (Fig. 2) of **2** was dominated by intense spin-allowed π–π* ligand-centered (LC) transitions, superimposed to anthracene-based $^1L_a$ transitions, in the UV region and by moderately intense spin-allowed metal-to-ligand charge-transfer (MLCT) transitions in the visible, which extend throughout the entire visible region. The lowest energy absorption feature (a shoulder at about 620 nm) is assigned to the Ru-to-molecular strand CT transition, where the acceptor ligand is mainly centered on the twice-coordinated, metal-bridging pyrimidine ring [11]. At room temperature in fluid solution, the molecular rack **2** exhibited a weak emission in the near-IR (Fig. 2), maximizing at 845 nm, with a lifetime of 60 ns and quantum yield of the order of $10^{-4}$ (see Table 1). The emission was assigned to the triplet MLCT state involving a bridging molecular strand orbital as the acceptor [11]. Luminescence of Ru(II) polypyridine complexes based on terpy-like ligands is usually inhibited at room temperature by a excited-state thermally-activated surface crossing process, populating a upper-lying metal-centered (MC) state [9], however the low energy of the lowest-lying MLCT state in **2**, a consequence of the less negative reduction potential of the coordinated molecular strand, decreases the efficiency of the thermally-activated decay process and allows luminescence to be detected, although with a low

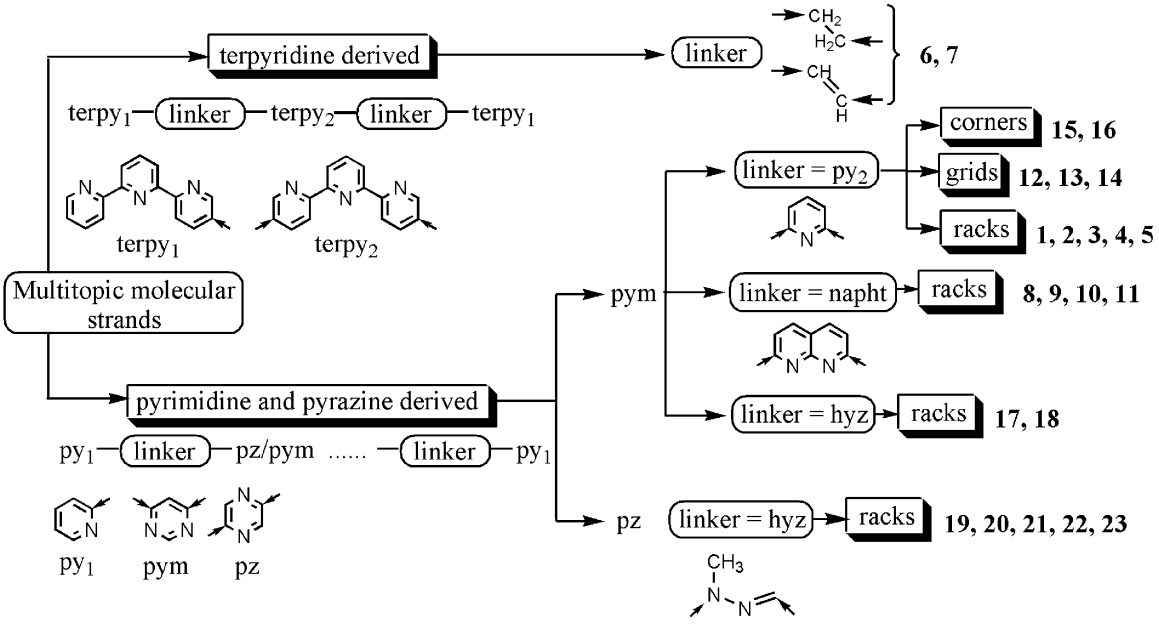


Scheme 1. General schematization of the various synthetic procedures for the compounds discussed in this article. For details, see in the text.

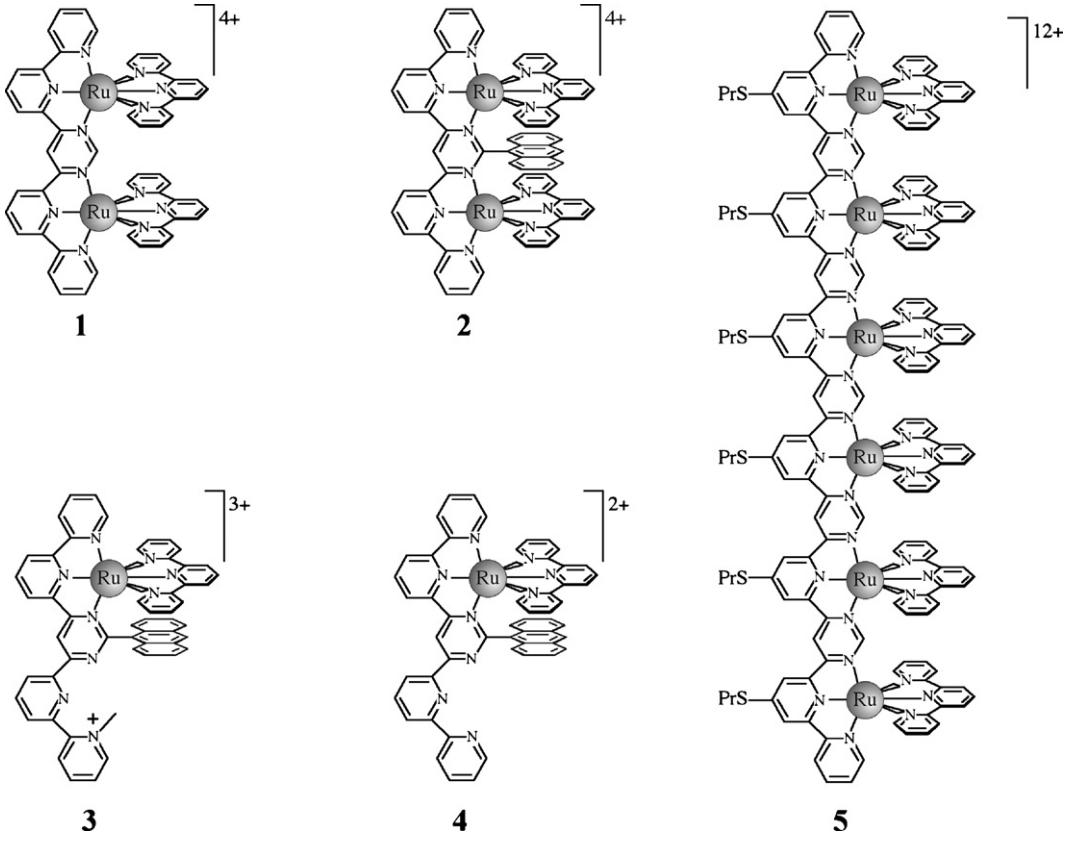


Chart 1. Structural formulae of **1**–**5**. The compounds shown here, as well as all the other cationic species reported in this article, have been synthesized as hexafluorophosphate salts.

quantum yield. At 77 K in rigid matrix, the thermally-activated decay process is inefficient and strong $^3$MLCT emission is recorded (emission maximum, 775 nm; lifetime, 1.6 μs, see Table 1) [11].

It can be noted that the presence of the anthracene subunit does not modify the properties of the lower, emitting $^3$MLCT state, as shown by the luminescence properties of **2**, which are very similar to those of **1** (Table 1). However, efficient energy transfer from the anthracene-centered excited states to the Ru-based MLCT state takes place. The role of the anthracene unit is therefore to enhance light absorption, particularly in the UV and in the 320–400 nm region, where the $^1L_a$ transition of the 9-substituted anthracene unit takes place [11]. Compound **2** can be seen as an example of light-harvesting molecular racks whose molecular strand structure contains additional chromophoric subunits.

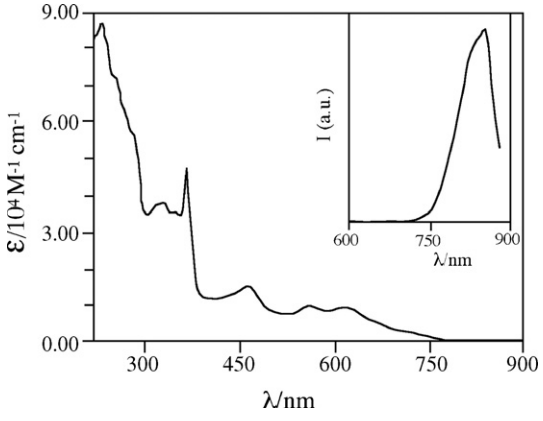


Fig. 2. Absorption and (inset) emission spectra of **2** in acetonitrile at room temperature.

The metal-centered oxidation processes in rack-type compounds as **1** and **2** are split (Table 1), so indicating a significant electronic interaction between the metal center subunits, similarly to that occurring in other dinuclear ruthenium complexes [1,9]. Both first and second reduction processes in **1** and **2** involve the (bridging) molecular strands, which are easier to reduce than the two terpyridine ligands. The terpyridine ligands are reduced at different potentials (see Table 1, reduction data of **2**), indicating noticeable electronic coupling between them, operating most likely by through space interactions.

Two compounds derived from **2**, the monometallic species **3** and **4** (see Chart 1) [12], where one of the two chelating sites of the bis(bipyridine)pyrimidine strand is set free and not used for metal coordination, exhibit emission from the MLCT state(s) involving the bis(bipyridine)pyrimidine strand as the acceptor at room temperature (emission energy at 730 and 715 nm for **3** and **4**, respectively, substantially higher than emission of **2**, since the pyrimidine is only mono-coordinated; lifetime in the ns timescale and quantum yields in the $10^{-2}$ to $10^{-3}$ range, see Table 1), and emission from the lowest-lying triplet anthracene state at 77 K in rigid matrix (emission energy, 685 nm, lifetime in

Table 1
Spetroscopic, luminescence and redox data of molecular racks based on poly(pyridine-pyrimidine) and tris-terpyridine strands

| | Absorption[a] $\lambda_{max}$ (nm) ($\varepsilon$, $M^{-1}\,cm^{-1}$) | Luminescence, 298 K | | | Luminescence (77 K[b]) | | Redox data[c] V vs. SCE | | Reference |
|---|---|---|---|---|---|---|---|---|---|
| | | $\lambda_{max}$ (nm) | $\tau$ (ns) | $\Phi$ | $\lambda_{max}$ (nm) | $\tau$ (μs) | $E_{1/2}$ (ox) | $E_{1/2}$ (red)[d] | |
| **1** | 615 (9500) | 845 | 60 | $5 \times 10^{-4}$ | 770 | 1.8 | +1.41, +1.57 | −0.43; −1.03; −1.56 stripping | [5], [e] |
| **2** | 620 (9000) | 845 | 60 | $5 \times 10^{-4}$ | 775 | 1.6 | +1.41, +1.58 | −0.45; −1.07; −1.52; −1.58 | [5,11] |
| **3** | 530 (7600) | 730 | 60 | $4.1 \times 10^{-3}$ | 685 | 510 | [f] | [f] | [12] |
| **4** | 510 (11500) | 715 | 30 | $1.5 \times 10^{-3}$ | 685 | 680 | [f] | [f] | [12] |
| **5** | 660 (55000) | – | – | – | 840 | [f] | +1.45 [2][g] | [h] | [13] |
| **6** | 475 (36000) | – | – | – | 608 | 9.4 | [f] | [f] | [14] |
| **7** | 479 (34000) | 690 | 11 | $7 \times 10^{-5}$ | 620 | 1.6 | [f] | [f] | [14] |

Data are in deaerated acetonitrile, unless otherwise stated.
[a] Only the lowest-energy spin-allowed MLCT band maximum is given.
[b] In butyronitrile rigid matrix.
[c] The processes are reversible or quasi-reversible. The number in square brackets indicates the number of exchanged electrons; when this number is not indicated, the process is monoelectronic.
[d] Only the first two reduction processes are reported.
[e] Luminescence data not previously published.
[f] Not studied.
[g] This process is assigned to the almost simultaneous one-electron oxidation of the two peripheral metal centers.
[h] Overlapping waves.

the $10^{-4}$ to $10^{-3}\,s^{-1}$, Table 1). As a consequence, the *direction* of the electronic energy transfer (from the anthracene to the metal-based subunit or vice versa) could be controlled in these species by temperature and/or rigidity of the medium [12].

Larger Ru(II) molecular racks based on poly(pyridine-pyrimidine) strands have been prepared [13]. The largest species of this series is **5** (Chart 1), based on a hexatopic molecular strand. The photophysical properties of this species have not been studied in full detail yet, anyway it does not exhibit luminescence at room temperature, while the usual MLCT emission takes place in a glass at 77 K (emission maximum at wavelength longer than 800 nm) [13].

## 3. Linearly-arranged multinuclear Ru(II) complexes based on tris-terpyridine strands

The two species, **6** and **7** (Chart 2), reported in this chapter strictly speaking are not molecular racks, since their structure is not perfectly determined (the molecular strand is not rigid), however they are included in this overview since they share with the molecular racks a linear sequence of Ru(II) chromophores. Compounds **6** and **7** are based on molecular strands containing three terpy-like chelating sites, differently substituted and connected each other [14]. In spite of their apparent similarity, **6** and **7** exhibit somewhat different photophysical properties (see Table 1, Fig. 3): **6** shows emission only at 77 K in rigid matrix (maximum at 608 nm; lifetime, 9.4 μs), while **7** emits both at room temperature in fluid solution (emission maximum, 690 nm; lifetime, 11 ns; quantum yield, $7 \times 10^{-5}$) and at 77 K in rigid matrix (emission maximum, 620 nm; lifetime, 1.6 μs) [14]. The difference in the luminescence properties of the compounds is due to the different substituents of the terpy ligands. In **6**, only electron donor substituents are present: the lowest MLCT state of the whole assembly is the MLCT triplet state involving the central Ru(II) center and its unsubstituted terpy ligand, and this is the state from which emission takes place. In **7**, also

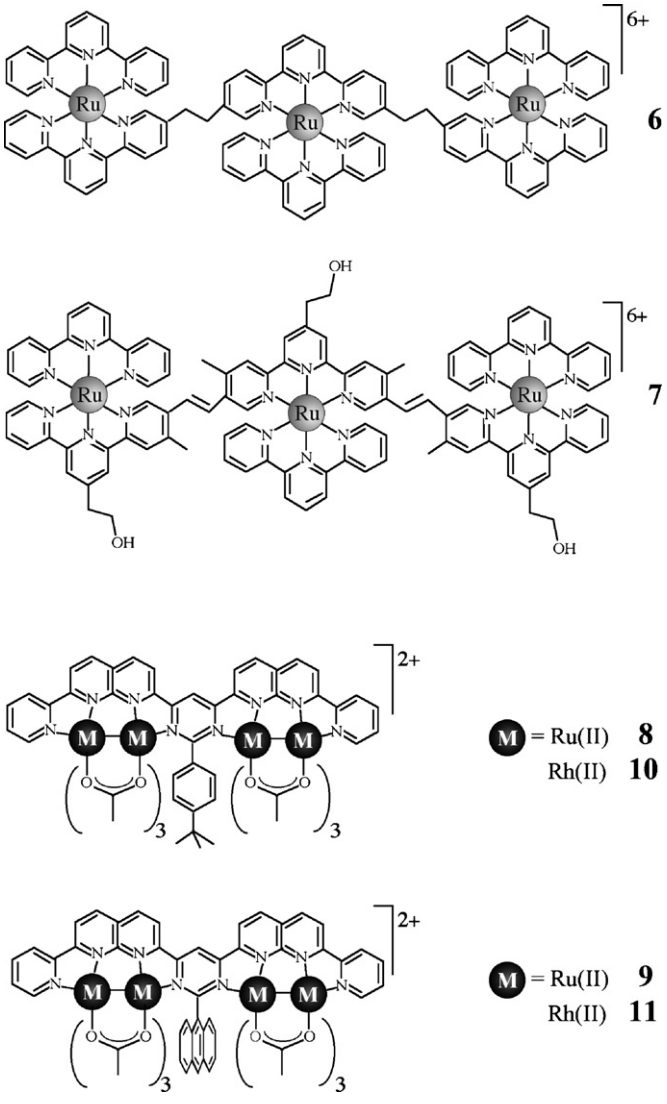


Chart 2. Structural formulae of **6**–**11**.

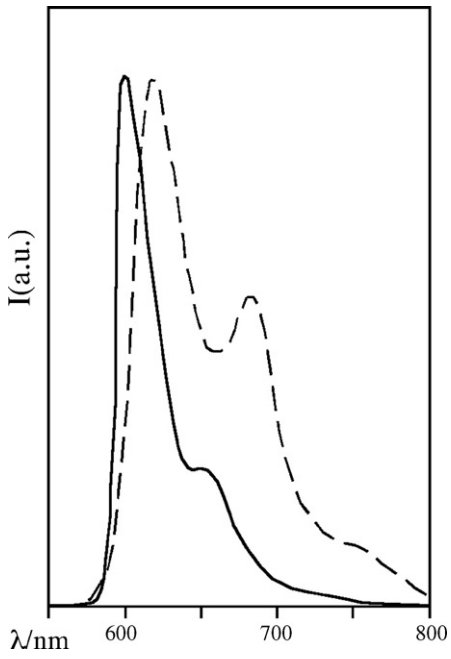


Fig. 3. Luminescence spectra of **6** (solid) and **7** (dashed) in butyronitrile matrix at 77 K.

electron acceptor substituents are present (i.e., the –CH=CH– moieties connecting the terpys on the molecular strand), and apparently the electron acceptor substituents effect dominates. The lowest-lying, emitting MLCT state of **7** actually involves the central, pentasubstituted terpy belonging to the molecular strand. The lowest-lying MLCT excited state of **7** is displaced to lower energy than that of **6**, and in the former species the above mentioned thermally-activated decay process (via population of the upper-lying MC state) is less efficient than in the latter, allowing emission to take place also at room temperature. In both **6** and **7**, a unique emission is always found (i.e., the emission is excitation wavelength independent and the decay is strictly monoexponential), suggesting that energy transfer from the peripheral chromophores to the central one occurs [14].

## 4. Molecular racks containing naphthyridine units

Molecular racks containing metal–metal bonded systems as subunits have been prepared by inserting naphthyridine moieties within the molecular strands [15]. The bis-diruthenium compounds **8** and **9** have been synthesized and studied, together with the analogous bis-dirhodium compounds **10** and **11** (see Chart 2) [16]. Beside the extension of the molecular rack structure to include a variety of building blocks apart the most studied metal polypyridine complexes, the interest in these species was driven by the known redox properties of the metal–metal bonded systems [17]. These properties opened the possibility of designing novel mixed-valence species having molecular rack structure and based on metal–metal bonded dimetallic subunits, yet unknown at the time: moreover, such mixed valence species could in principle to be formed at milder potential than molecular racks based on formerly prepared poly(pyridine-pyrimidine) strands. Actually, while metal-centered oxidations of the "classical" subunits of complexes **1**–**7** occur in the potential window +1.20/+1.60 V (vs. SCE) [5,14], the oxidation of each metal-metal bonded diruthenium subunit of **8** and **9** occurs in the +0.70/+0.90 V potential window [16]. The observation of two distinct oxidation potentials for the two $M_2$ units in **8**–**11** indicated a non-negligible electronic interaction between the two metal–metal bonded dimetallic subunits of the four complexes (see Table 2) and allowed the study of relatively stable mixed-valence species [16]. Interestingly, the oxidation splitting was larger for **9**, containing the anthryl group (0.13 V) than for **8**, containing the substituted phenyl moiety (0.09 V). This result highlights the effect of through–space interaction

Table 2
Absorption spectra and redox data of molecular racks containing naphthyridine units and molecular grids, including mononuclear precursors

| | Absorption[a] $\lambda_{max}$ (nm) ($\varepsilon$, $M^{-1}$ $cm^{-1}$) | Redox data[b] V vs. SCE | | Reference |
|---|---|---|---|---|
| | | $E_{1/2}$ (ox) | $E_{1/2}$ (red)[c] | |
| **8** | 695 (4200) | +0.76; +0.85 | −0.31 | [16] |
| **9** | 701 (4200) | +0.73; +0.86; +1.51irr[d] | −0.30 | [16] |
| **10** | 622 (3700) | +1.43; +1.50 | −0.21 | [16] |
| **11** | 634 (3800) | +1.32; +1.53irr [2][e] | −0.18 | [16] |
| **12** | [f] | +1.32; +1.38; +1.67 | −0.27; −0.32; −0.46; −0.51; −1.07; −1.17; −1.35[g] | [19] |
| **13** | [f] | +1.35; +1.40: +1.59; +1.76 | −0.25; −0.32; −0.46; −0.52; −1.09; −1.19; −1.38; −1.46 | [19] |
| **14** | [f] | +1.15 [2]; +1.53 [2] | −0.30 [2]; −0.51; −0.57; −1.04; −1.15 | [19] |
| **15** | 543 (18190) | +1.31 | −0.85; −1.02; −1.52; −1.60[g] | [19] |
| **16** | 549 (19570) | +0.96 | −0.81; −1.03; −1.54; −1.82[g] | [19] |

Data are in acetonitrile, unless otherwise stated.
[a] Only the lowest-energy spin-allowed MLCT band maximum is given.
[b] The processes are reversible or quasi-reversible. The number in square brackets indicates the number of exchanged electrons; when the number of exchanged electrons is not indicated, the process is monoelectronic.
[c] For complexes **8–11**, further ill-behaved reduction processes take place.
[d] This process is assigned to anthracene-based oxidation.
[e] This process involves both metal-centered and anthracene-based oxidation.
[f] Not reported.
[g] Adsorption on the electrode.

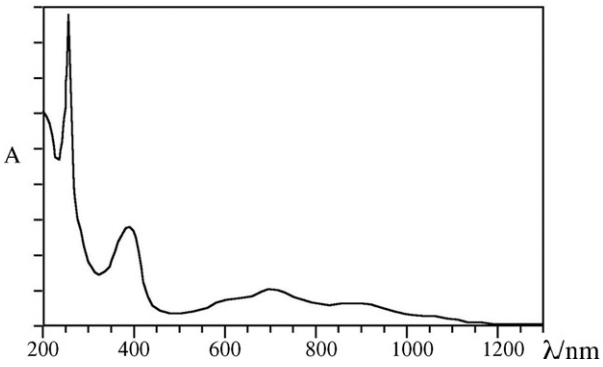


Fig. 4. Absorption spectrum of **9** in acetonitrile.

in mediating electronic interaction. Indeed, it is assumed that electronic coupling between the identical redox-active subunits of dinuclear metal polypyridine complexes, as well as of the metal–metal bonded dimetallic subunits of **8**–**11**, are dominated by through-bond superexchange involving the LUMO of the bridging ligands (in the case of molecular racks under discussion, such LUMO would mainly be based on the pyrimidine moieties) [16]. The anthracene group may contribute to the electronic coupling between the redox sites by opening a new pathway to superexchange, for example mediating a through–space interaction involving anthracene-based orbitals. The redox data shows ~~as~~ an anthracene-based oxidation at about 1.50 V vs. SCE (see Table 2), which indicate that the anthracene-based HOMO is close in energy to the metal-centered orbitals, so that a hole-transfer pathway involving anthracene HOMO is quite possible. The HOMO of the phenyl group is at lower energy and cannot contribute to the interaction. A more detailed discussion can be found in the original paper [16].

As far as the spectroscopic properties of the naphthyridine-based molecular racks are concerned, their absorption spectra are very rich, as expected because of the presence of several chromophoric units. The spectra of all the complexes (Table 2; for a representative example, see Fig. 4) show an intense absorption feature between 320 and 400 nm. This feature receives a large contribution from spin-allowed π–π* (LC) transitions involving the (bridging) molecular strands. In the anthryl-containing species, contribution from the spin-allowed anthracene-centered $^1L_a$ transitions is obscured by molecular strand-based transitions, whereas the stronger $^1B_a$ transition at about 254 nm is clearly showed. In the visible region, the lowest-energy band is attributed to a charge transfer transition from each dimetallic subunit (most likely, from a π* orbital extending over the two metal centers) to the (bridging) molecular strand. Such a transition can be named metal–metal to ligand charge transfer ($M_2$LCT) transition because of the strong interaction between the metal–metal bonded units of each component. The absorption bands the bis-diruthenium racks are red-shifted compared to the dirhodium species, with the lowest-energy band of **8** and **9** extending into the near-IR region, in agreement with the $M_2$LCT assignment, since the metal-based HOMOs of the ruthenium compounds are higher in energy (and therefore their oxidation potentials are less positive) than those of the corresponding rhodium species (see Table 2) [16].

None of the four naphthyridine-based racks **8**–**11** exhibits any luminescence either at room temperature or at 77 K. This agrees with the excited-state properties of metal–metal bonded acetate species, which are known to deactivate by radiationless transitions. However, one of the bis-dirhodium racks, **10**, exhibits a long-lived (lifetime, 5.8 μs) transient absorption spectrum, indicating that the excited state can be efficiently involved in bimolecular processes [16].

## 5. Molecular grids

Within the field of supramolecular coordination chemistry, the natural evolution of molecular rack-type systems is the design of grid-type compounds [3,18]. Molecular grids can indeed be considered as the three-dimensional analogues of the one-dimensional rack-type compounds, where ladder-type compounds represent the two-dimensional systems (Fig. 5). The photophysical properties and redox behavior of the heterometallic [2 × 2] molecular grid **12**, made of two Ru(II) and two Fe(II) subunits, has been studied, together with the same properties of the homometallic Fe(II) grid **13**, of the heterometallic Os-Fe grid **14**, and of the monometallic precursors **15** and **16** (see Chart 3 for the structures) [19].

The absorption spectra of **12**–**16** exhibit the typical feature of Fe(II), Ru(II), and Os(II) polypyridine complexes, that is strong LC bands in the UV region and intense MLCT bands in the visible, which extend towards the near IR region (Fig. 6). The monometallic **15** and **16** precursors exhibit the typical $^3$MLCT emission, both at room temperature and at 77 K (298 K, acetonitrile: **15**: $\lambda_{max} = 720$ nm, $\tau = 59$ ns, $\Phi = 2.4 \times 10^{-3}$; **16**: $\lambda_{max} = 825$ nm, $\tau = 18$ ns, $\Phi = 1.8 \times 10^{-3}$; 77 K, butyronitrile matrix: **15**: $\lambda_{max} = 685$ nm, $\tau = 4.95$ μs; **16**: $\lambda_{max} = 820$ nm, $\tau = 630$ ns) [19], whereas the grids **12**–**14** do not exhibit luminescence. The absence of luminescence of the three grids was expected since all of them contain Fe(II) subunits, whose lowest-lying excited-states, of MC nature, are known to deactivate via nonradiative transitions. Apparently, the potentially luminescent MLCT states involving the Ru(II) and Os(II) subunits are efficiently quenched in the grid by intercomponent electronic energy transfer populating the MC states involving the iron(II) subunits.

All the three molecular grids here reported exhibit a very rich and interesting electrochemistry (Table 2), which yields several pieces of information of the electronic structure and interactions of the various subunits [19]. As an example, for the sake of sim-

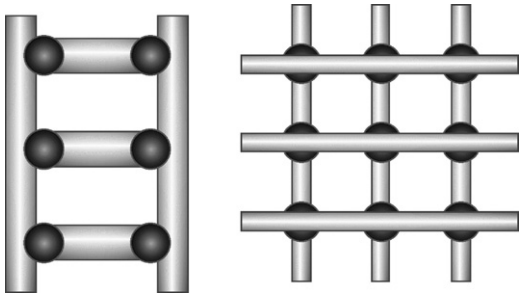

Fig. 5. Schematic representation of ladders (left) and grids (right).

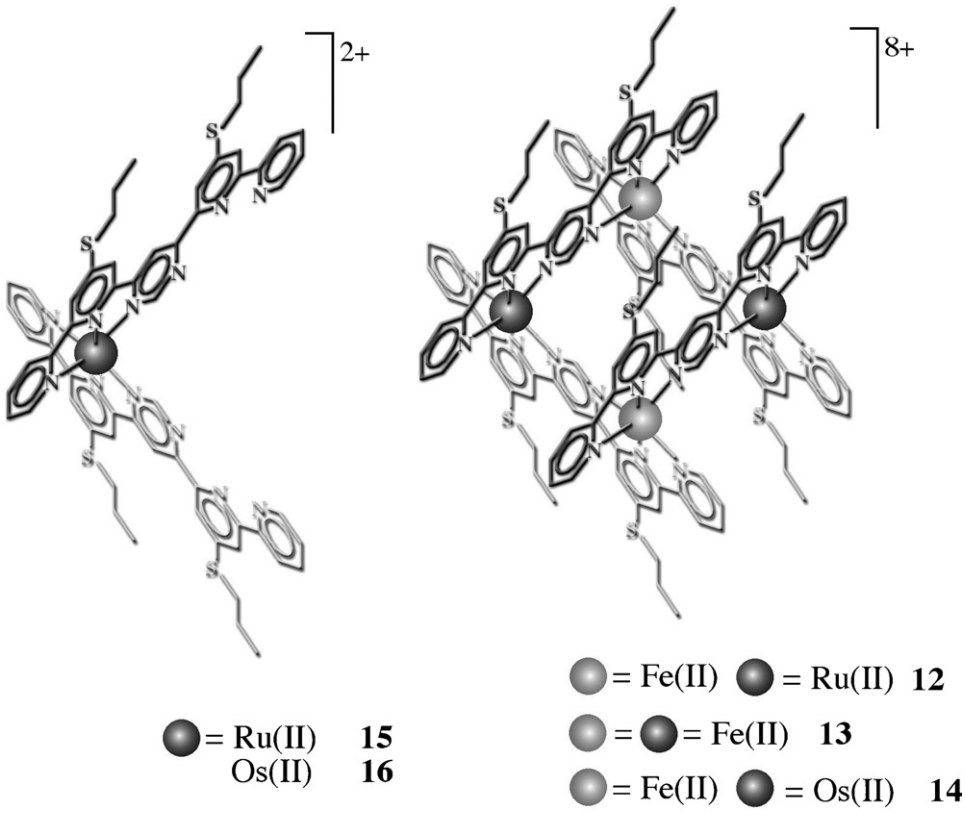


Chart 3. Structural formulae of **12**–**16**.

plicity here we report in some detail the redox properties of the homometallic Fe(II) [2 × 2] grid **13**, where the interpretation of the results is not complicated by the presence of different metal subunits and therefore is more informative of the various electronic interactions as mainly due to the grid structure. However, similar qualitative conclusions where also drawn by analyzing the behavior of the heterometallic grids [19].

The molecular grid **13** (Table 2, Fig. 7) undergoes four monoelectronic reversible oxidation processes, which are assigned to the four metal-centered orbitals. Following the first oxidation of one of the four identical metal centers, a second oxidation process is observed at a potential only slightly more positive than the first ($\Delta E_{1/2}$ = 50 mV). Because the redox data of dinuclear Ru(II) complexes containing a bridging pyrimidine ring indicate that there is significant electronic interaction between metal centers connected to the same (bridging) molecular strand (for example, $\Delta E_{1/2}$ = 300 mV for **2** [5]), it can be concluded that the second oxidation process involves the Fe(II) center which is farthest away, that is diagonal to the first oxidized center (Fig. 7). The third oxidation process concerns one of the two other Fe(II) centers. Its potential is significantly more positive than the second one ($\Delta E_{1/2}$ = 190 mV), in agreement with the presence of two nearby (formally) Fe(III) centers. The fourth oxidation involves of course the remaining Fe(II) center [19].

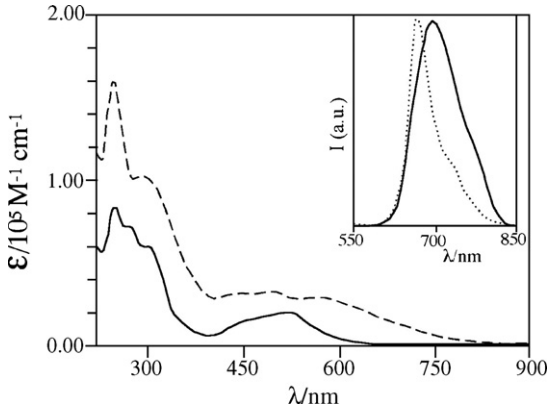


Fig. 6. Absorption spectra of **15** (solid) and **12** (dashed) in acetonitrile. Inset: luminescence spectra of **15** in acetonitrile, room temperature (solid) and in butyronitrile, 77 K (dotted).

The separation of the third and fourth oxidation processes (170 mV), which depends on the electronic interactions between two opposite corners of the molecular grids when the other corners are Fe(III) centers, is larger than the separation between the first two processes (50 mV), which depends on the electronic interactions between two opposite corners of the molecular grids when the other corners are Fe(II) centers. Such a difference clearly indicates that *the electronic interaction between two redox-active sites localized at opposite corners of* ***13*** *is a function of the oxidation state of the other redox-active sites*.

As far as the reduction behavior is concerned, the first reduction of **13** involves a ligand orbital which receives a large contribution from the pyrimidine ring: such aryl ring, beside having its LUMO lower than those of the pyridine rings, is also coordinated by two (positively-charged) metal centers. The second reduction takes place at a potential that is more negative by 70 mV. Because the interaction between two identical ligands

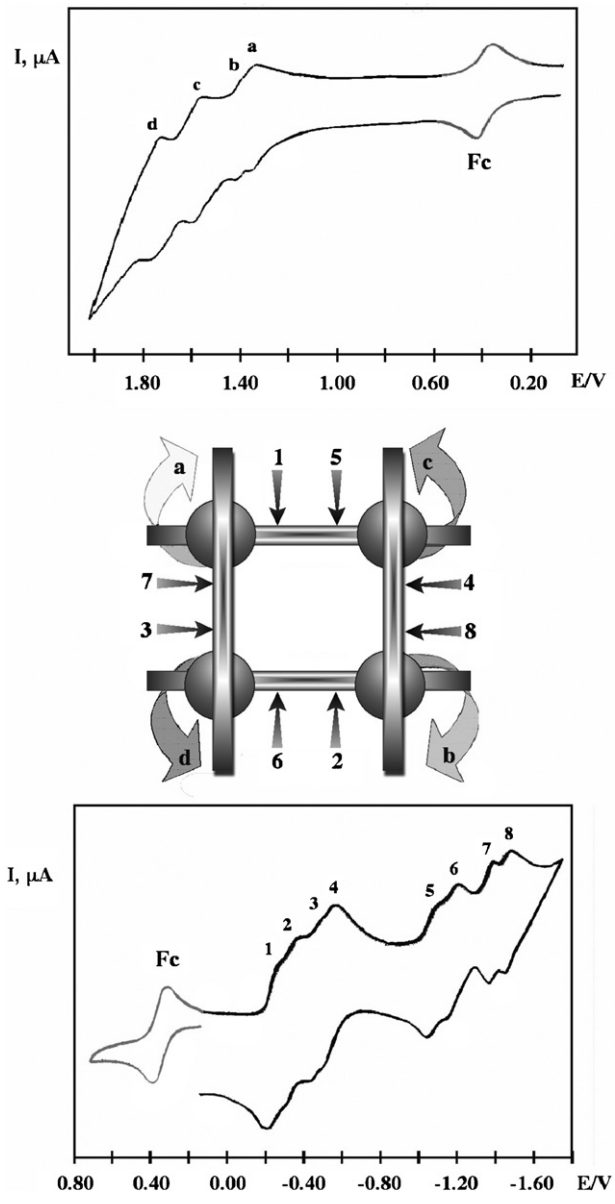


Fig. 7. Redox behavior of **13**: cyclic voltammetry curves in acetonitrile vs. SCE (top, oxidation; bottom, reduction). In the middle, assignment of the various oxidation (a–d) and reduction (1–8) processes is reported. Fc stands for ferrocene, used as an internal reference [19].

coordinated to the same metal center in these complexes can be inferred by the separation between the two first reduction processes of the mononuclear precursor species **15** and **16** (about 200 mV), the relatively small difference in potential between the first two reduction processes of the grid **13** suggests that the second reduction involves the bridging ligand which is opposite to the first one (Fig. 7). On the basis of the above discussion, the third and fourth processes are assigned to one-electron reduction of the other two bridging ligands. The separation between the second and third processes (140 mV) and third and fourth ones (60 mV) supports the assignment and highlights the dependence of the electronic interaction between ligands on their relative location in the grid. At potentials more negative than −1.00 V, **13** exhibits four additional, quasi-reversible processes. These are assigned to the second one-electron reduction of each ligand, following the same sequence of the first four processes.

The results obtained, which are also in agreement with those reported for other [2 × 2] grids based on different metals [20,21], indicate that in molecular grid structures as the ones studied, significant interaction among the various subunits takes place, however any redox process can be assigned to specific component of the supramolecular structure. Because of their redox properties, theses molecular grids are very attractive as molecular storage devices: in the case of **13**, for example, 12 different reversible redox states at relatively mild potentials can be obtained. The combination of structure and redox properties also suggests that such species could be suitable to experimentally test the concept of cellular automata [3b,22]. Moreover, they are attractive systems for light-harvesting purposes, as it was demonstrated that the light energy absorbed by any specific metal-based component is very efficiently channeled to the metal center subunit(s) where the lowest-energy excited state of the whole multicomponent system is localized (for **12** and **14**, the Fe(II)-based MC state).

## 6. Ruthenium(II) molecular racks made of polytopic hydrazone-based molecular strands

On the search for facile and efficient synthetic pathways to polytopic molecular strands, the 2,6-disubstituted pyridine ring ($py_2$) of the molecular strands used in formerly discussed systems was replaced by its isomorphic equivalent, a hydrazone (hyz) group [7a,7b]. This also allowed to increase the molecular diversity (Fig. 8): for a ligand strand with two tridentate terpy-like sites ($py_1$-$py_2$-pym-$py_2$-$py_1$; $py_1$ is a 2-mono-substituted pyridine, the terminal ring of the strand, and pym is the central 4,6-disubstituted pyrimidine), replacing $py_2$ by a hydrazone group generates two types of 2-sites symmetric isomeric ligands, because the central unit may be derived from a bis(hydrazino)pyrimidine or from a pyrimidine-dicarboxaldehyde. This isomerism implies the change of the position of the C=N bond. Thus, one gains synthetic efficiency and simplicity, but also access to diverse molecular species, that is to two possibilities for py-hyz-pym-hyz-py **a** and **b**, instead of one for $py_1$-$py_2$-pym-$py_2$-$py_1$ (see Fig. 8). The same synthetic strategy was applied to other 2-sites ligands, such as the $py_1$-$py_2$-pz-$py_2$-$py_1$ (pz = 2,5-disubstituted pyrazine) sequence [23], whose hydrazone analogues **c** and **d** have also been prepared (Fig. 8).

By using the molecular strands **a**–**d**, the four dinuclear molecular racks 17–20 (Chart 4) have been synthesized and their spectroscopic, photophysical and redox properties have been studied [24,25]. Table 3 collects the spectroscopic and redox data, and Fig. 9 shows the absorption and emission spectra of **17** and **18**. The results indicate that the different topologies, in particular the position of the C=N group and the nature of the central ring (pyrimidine vs. pyrazine), translate into significant differences in the structural and electronic properties of the hydrazone-based molecular racks.

The first obvious structural difference between the species containing a pyrimidine ring, i.e. **17** and **18**, and the species

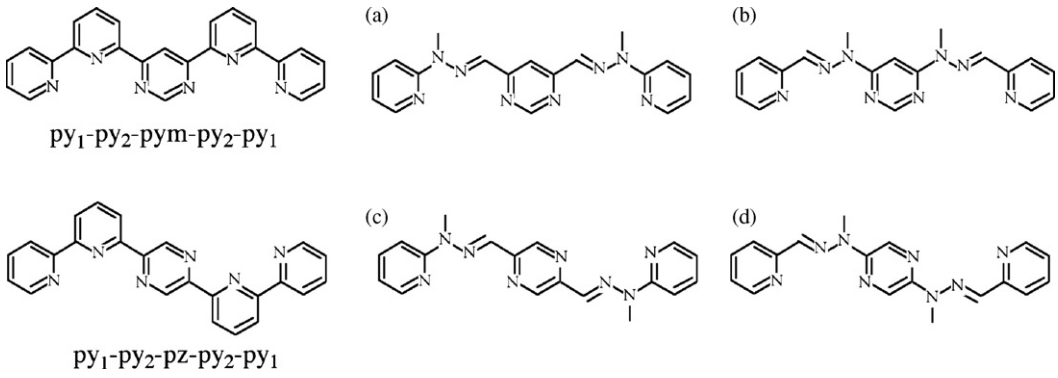


Fig. 8. Some molecular strands discussed in the text.

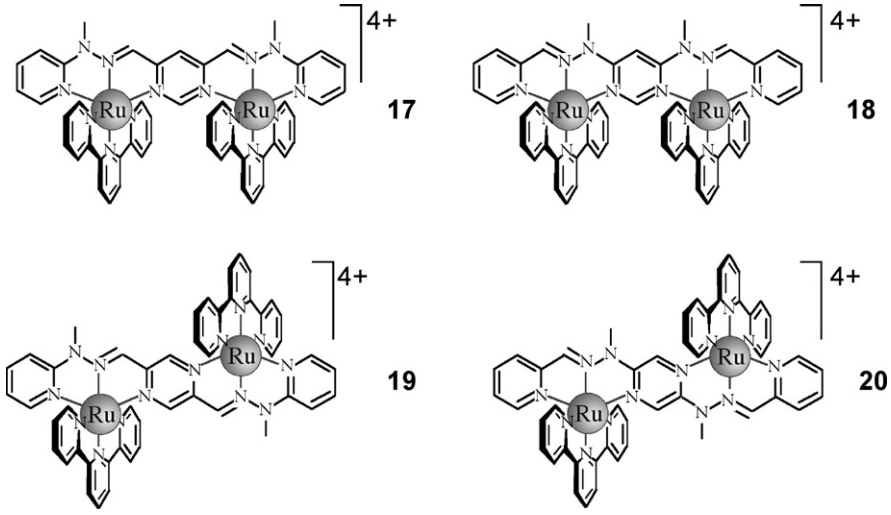


Chart 4. Structural formulae of **17**–**20**.

containing the pyrazine ring, **19** and **20**, is that the Ru(terpy)$^{2+}$ moieties of the racks are on the same side with respect to the molecular rack main axis in the case of the pyrimidine-containing systems, whereas they lie on opposite sides in the case of the pyrazine-containing systems, so generating "alternate" racks (see Chart 4). Moreover, the molecular racks **17** and **18** exhibit a bent structure, whereas **19** and **20** are effectively linear (Fig. 10) [24]. As far as the position of the C=N group in the

Table 3
Absorption, luminescence and redox data of hydrazone-based molecular racks, in deaerated acetonitrile solution, unless otherwise stated

| | Absorption[a] $\lambda_{max}$ (nm) ($\varepsilon$, $M^{-1}$ $cm^{-1}$) | Luminescence, 298 K $\lambda_{max}$ (nm) ($\tau$, ns) | Luminescence, 77 K[b] $\lambda_{max}$ (nm) ($\tau$, ns) | Redox[c] V vs. SCE | | Reference |
|---|---|---|---|---|---|---|
| | | | | $E_{1/2}$ (ox) | $E_{1/2}$ (red) | |
| **17** | 630 (27000) | [d] | [d] | +1.36; +1.66 | −0.45; −1.05; −1.46; −1.65 | [24] |
| **18** | 470 (20700) | 758 (30) | 741 (335) | +1.28; +1.53; +1.78[e] | −0.98; −1.22; −1.35 | [24] |
| **19** | 614 (40600) | [d] | [d] | +1.27; +1.50 | −0.50; −1.05; −1.49; −1.57 | [24] |
| **20** | 468 (21200) | 750 (40) | 734 (390) | +1.27; +1.52 | −0.88; −1.32; | [25] |
| **21** | [f] | [d] | [d] | +1.30; +1.43 | [f] | [26] |
| **22** | [f] | [d] | [d] | +1.32; +1.37; +1.61[g] | [f] | [26] |
| **23** | [f] | [d] | [d] | +1.34 [2];[h] +1.43; +1.64irr | [f] | [26] |

[a] Only the lowest-energy spin-allowed MLCT band maximum is given.
[b] In butyronitrile rigid matrix.
[c] The processes are reversible or quasi-reversible. The number in square brackets indicates the number of exchanged electrons; when the number of exchanged electrons is not indicated, the process is monoelectronic. On reduction, other processes occur at more negative potentials for all the complexes.
[d] No emission at wavelength shorter than 850 nm.
[e] This oxidation process most likely involves molecular strand subunits centered on the methyl-amino groups.
[f] Data not available yet.
[g] Process involving inner metal centers.
[h] This process is the almost simultaneous one-electron oxidation of both peripheral metal centers.

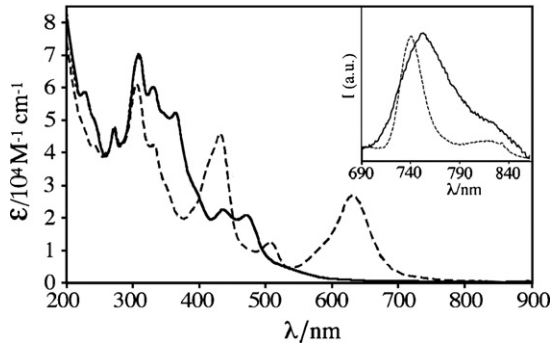


Fig. 9. Absorption spectra of **17** (dashed) and **18** (solid) in acetonitrile and (inset) luminescence spectra of **18** in acetonitrile at 298 K (solid) and in butyronitrile at 77 K (dashed).

molecular frame is concerned, from reduction potential values (Table 3), and considering that the first reduction involves in all the cases an orbital mainly centered on the twice-metalled pyrimidine/pyrazine ring, it can be inferred that when the C=N groups are directly linked to the central pyrimidine/pyrazine ring (i.e., in **17** and **19**) a very low-lying LUMO is present and delocalized over both the C=N groups and the central aryl ring, whereas when a methyl amino group is interposed between each C=N group and the pyrimidine/pyrazine central ring (as in **18** and **20**), the LUMO lies at much higher energy and is essentially centered only on the twice-matallated aryl ring. Such a large difference in the LUMO energy is also responsible for the localization of the second reduction process in the four racks, which in **17** and **19** is still centered on the bringing molecular strand, whereas in **18** and **20** involves a terpy ligand [24].

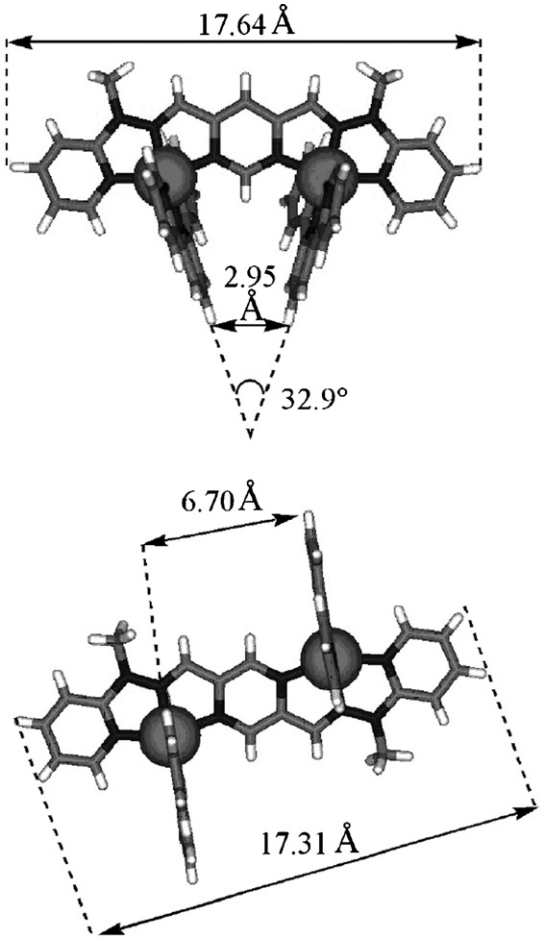


Fig. 10. X-ray structures of **17** (top) and **19** (bottom) [24].

The presence of very low-lying LUMOs in **17** and **19** also leads to MLCT states at low energy: this is showed in **17** and **19** by strong visible bands, due to spin-allowed MLCT transitions, in the 500–700 nm range (see Table 3, Fig. 9). In **18** and **20**, in agreement with the reduction data, the corresponding MLCT bands are found at much higher energies, with maxima at wavelengths shorter than 500 nm. Luminescence from $^3$MLCT states is found for **18** and **20** in the 720–800 nm energy range (Fig. 9, Table 3), whereas emission from analogous states of **17** and **19** is expected at energies lower than 850 nm, and in fact is not detected with usual fluorimeters and photomultipliers, for which sensitivity becomes extremely low at $\lambda > 850$ nm. Near IR luminescence experiments with suitable detectors for hydrazone-based molecular racks have not been reported yet.

Larger Ru(II) hydrazone-based molecular racks, containing three (**21**), four (**22**), and six (**23**) metal subunits have been reported (see Chart 5) [26]. In all these species, pyrazine rings are present within the molecular strand framework. Absorption spectra and photophysical properties of **21**–**23** have not been reported yet, however quite interesting oxidation properties have been communicated (Table 3) [26]. Indeed, the molecular racks **21**–**23**, together with their smaller analogue **20**, represent an homologous series of "modular" compounds, in which the separation between the peripheral, roughly identical meta-based subunits increases along the series by the presence of an increasing number of intermediate metal-based subunits which plays the role of spacers. The metal subunits easier to be oxidized in **21**–**23** are the terminal subunits. In fact, the inner subunits are more difficult to be oxidized compared to the terminal ones because of the different coordination environment (e.g., the peripheral metal centers are coordinated by one pyridine and by only one bridging pyrazine ring, while the inner metal centers carry two bridging pyrazine, which are known to be stronger electron withdrawing groups than the terminal pyridine rings). However, the first two oxidation processes in **21** and **22** are both monoelectronic, indicating splitting of the peripheral metal-based oxidation process, similarly to that which occurs, obviously, in **20**, where no intermediate inner metal center is present. The sizeable splitting of the oxidation potential of the peripheral (outer) metal center subunits in **21** and **22** has no precedent in Ru(II) multinuclear complexes with nuclearity larger than two, with the exception of molecular grids, which have a peculiar structure, and of complexes made of particular tritopic ligands like hexaazatriphenylene ligands [27]. This indicates that in the molecular racks **21**–**23** the inner metal-based subunits allow a significant electronic interaction between the outer subunits. The oxidation splitting is found to follow an exponential dependence on the outer metal center distance, as expected in the assumption that such an oxidation splitting is proportional to the effective electronic coupling between the

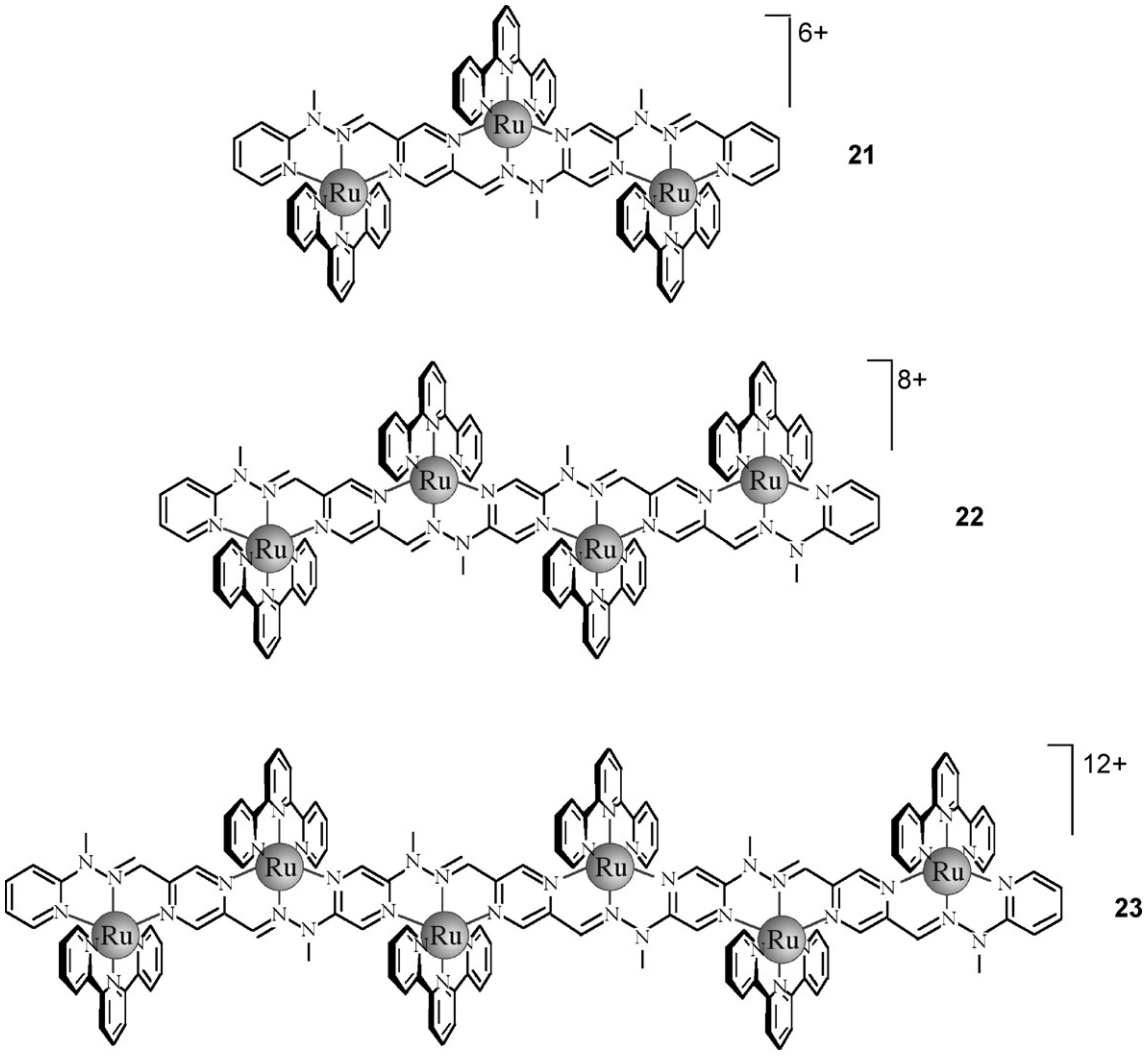


Chart 5. Structural formulae of **21**–**23**.

outer subunits [26]. The linear relationship shown in Fig. 11 and related to Eq. (1),

$$\ln H' = \ln H'(0) - \left(\frac{\beta}{2}\right)(r - r_0) \quad (1)$$

where $H'$ is half of the oxidation splitting, $H'(0)$ is related to the oxidation splitting for the interaction at the "contact" distance $r_0$ (no interposed units; in our case, it would be the splitting of the dinuclear system **20**), $r$ is the edge-to-edge distance between the peripheral subunits (calculated by using X-ray parameters of dinuclear systems [24]), and $\beta$ is the distance attenuation term for the electronic interaction, largely a property of the interposed spacer "module" (although it also depends on the nature of the terminal subunits) – allows to calculate a value of 0.23 $Å^{-1}$ for $\beta$ in the hydrazone-based molecular racks. This value compares well with those calculated for other molecular spacers which are usually considered good "electronic conductors": it is smaller than those reported for most phenyl groups in organic systems ($\beta$ about 0.5 $Å^{-1}$) [28] and even smaller than those obtained from photoinduced energy transfer rate constants between Ru(II) and Os(II) subunits separated by polyphenylene spacers (0.32 $Å^{-1}$) [29] in mixed-metal dinuclear species and from spectroscopic measurements in olefin-bridged diruthenium and dialkylamino compounds (also 0.32 $Å^{-1}$) [30]. Such results suggest that the hydrazone-based molecular racks feature properties typical of a genuine "molecular wire" and are therefore of potential interest for implementation in supramolecular electronic devices.

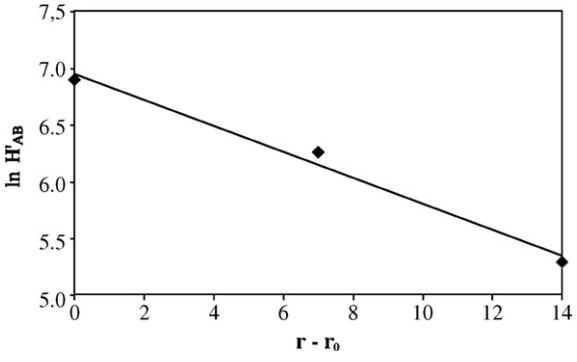


Fig. 11. Plot of Eq. (1) (see text).

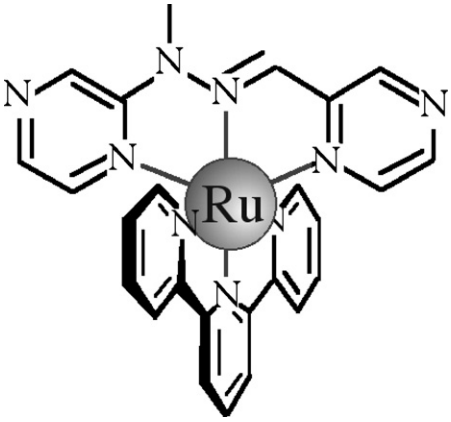


Fig. 12. The $\{$(pyrazine-hydrazone-pyrazine)Ru(terpy)$\}^{2+}$ spacer discussed in the text.

The molecular wire behavior exhibited by **20**–**23** warrants some additional comment. The low $\beta$ parameter featured by the $\{$(pyrazine-hydrazone-pyrazine)Ru(terpy)$\}^{2+}$ module (the individual inner subunit in **21**–**23**, see Fig. 12) contrasts with the much higher values implicitly found for the other types of metal-based "spacers" which are usually present in multicomponent Ru(II) systems [1a]. In fact, for such systems an oxidation splitting is not found (and a $\beta$ value cannot be calculated by the oxidation splitting method). For example, even in a molecular rack similar to **2** and **5**, but containing three metal centers, the oxidation of the two peripheral metal subunits occurs at the same potential, although the separation between the peripheral centers is smaller than in **22**, and close to that found in **21** [13]. It can be proposed that the better ability of the $\{$(pyrazine-hydrazone-pyrazine)Ru(terpy)$\}^{2+}$ building blocks to mediate electronic coupling, compared to that of the usual polypyridine-like Ru(II) subunits, is due to a superexchange-assisted interaction which take advantage of a hole-transfer mechanism. Redox studies performed on the free molecular strands **a**–**c** shown in Fig. 8 demonstrated that such species have relatively high energy HOMOs, mainly involving the methyl-amino groups [24]. Such HOMOs can couple with the metal-centered orbitals where oxidation takes place, and extend the electronic interaction throughout the molecular racks. Further studies are needed to confirm this suggestion.

## 7. Conclusions

The molecular racks and related grids discussed in this review article are quite interesting by many viewpoints. The properties of individual metal components are carried to a large extent in the supramolecular multicomponent systems. Absorption, emission, and redox processes can be assigned to specific subunits of the arrays, however they depends on both the individual components and the structural organization. Moreover, some novel properties and functions, like molecular-wire behavior, redox sequences, and intercomponent energy transfer processes, origin from the supramolecular nature of the species.

Beside the synthesis of novel molecular rack species, intriguing by the theoretical viewpoint, future interesting work is also expected to involve spectroelectrochemistry of mixed-valence species and ultrafast spectroscopy, not yet performed on such species. These studies can help to shine light on the electronic coupling and the rates of electron and energy flow within the various metal-based subunits, with possible intriguing consequences on applicative aspects. On this basis, it can be stated that the study of the properties of molecular racks is still in its infancy, and surely will be an intense field of research in the next years.

## Acknowledgements

We thank MIUR (PRIN project no. 2006030320) and the University of Messina (PRA Project) for financial support.

## References

[1] (a) V. Balzani, A. Juris, M. Venturi, S. Campagna, S. Serroni, Chem. Rev. 96 (1996) 759;
(b) F. Scandola, C. Chiorboli, M.T. Indelli, M.A. Rampi, in: V. Balzani (Ed.), Electron Transfer in Chemistry, 3, Wiley-VCH, Weinheim, 2001, p. 337;
(c) P. Ceroni, G. Bergamini, F. Marchioni, V. Balzani, Prog. Polym. Sci. 30 (2005) 453;
(d) V. Balzani, G. Bergamini, S. Campagna, F. Puntoriero, Top. Curr. Chem. 280 (2007) 1, and references therein;
(e) V.W.-W. Yam, E.C.-C. Cheng, Top. Curr. Chem. 281 (2007) 269.
[2] V. Balzani, A. Credi, M. Venturi, Molecular Devices and Machines, Wiley-VCH, Weinheim, Germany, 2003.
[3] (a) J.-M. Lehn, Proc. Natl. Acad. Sci. U.S.A. 99 (2002) 4763;
(b) M. Ruben, J. Rojo, F.J. Romero-Salguero, L.H. Uppadine, J.-M. Lehn, Angew. Chem. Int. Ed. 43 (2004) 3644, and references therein.
[4] (a) V. Balzani, S. Campagna, G. Denti, A. Juris, S. Serroni, M. Venturi, Acc. Chem. Res. 31 (1998) 26;
(b) F. Puntoriero, F. Nastasi, M. Cavazzini, S. Quici, S. Campagna, Coord. Chem. Rev. 251 (2007) 536.
[5] G.S. Hanan, C.R. Arana, J.-M. Lehn, G. Baum, G. Fenske, Chem. Eur. J. 2 (1996) 1292.
[6] For pyridine-pyrimidine based helical ligands that upon metal coordination can yield molecular racks, see:
(a) G.S. Hanan, J.-M. Lehn, N. Kyritsakas, J. Fischer, J. Chem. Soc., Chem. Commun. (1995) 765;
(b) D.M. Bassani, J.-M. Lehn, G. Baum, D. Fenske, Angew. Chem. Int. Ed. 36 (1997) 1845;
(c) M. Ohkita, J.-M. Lehn, G. Baum, D. Fenske, Chem. Eur. J. 5 (1999) 3471.
[7] For hydrazone-based helical ligands, see:
(a) K.M. Gardinier, R.G. Khoury, J.-M. Lehn, Chem. Eur. J. 6 (2000) 4124;
(b) J.-L. Schmitt, A.-M. Stadler, N. Kyritsakas, J.-M. Lehn, Helv. Chim. Acta 86 (2003) 1598.
[8] For other types of ligands used to prepare Ru(II) racks, see also:
(a) D. Brown, S. Muranjan, Y. Jang, R. Thummel, Org. Lett. 4 (2002) 1253;
(b) D. Brown, R. Zong, R.P. Thummel, Eur. J. Inorg. Chem. (2004) 3269;
(c) R. Zong, R.P. Thummel, J. Am. Chem. Soc. 127 (2005) 12802;
(d) R. Zong, D. Wang, R. Hammitt, R.P. Thummel, J. Org. Chem. 71 (2006) 167.
[9] (a) T.J. Meyer, Pure Appl. Chem. 58 (1986) 1193;
(b) A. Juris, V. Balzani, F. Barigelletti, S. Campagna, P. Belser, A. von Zelewsky, Coord. Chem. Rev. 84 (1988) 85;
(c) J.-P. Sauvage, J.-P. Collin, J.-C. Chambron, S. Guillerez, C. Coudret, V. Balzani, F. Barigelletti, L. De Cola, L. Flamigni, Chem. Rev. 94 (1994) 993;
(d) L. De Cola, P. Belser, Coord. Chem. Rev. 177 (1998) 301.
[10] S. Campagna, F. Puntoriero, F. Nastasi, G. Bergamini, V. Balzani, Top. Curr. Chem. 280 (2007) 117.

[11] A. Credi, V. Balzani, S. Campagna, G.S. Hanan, C.R. Arana, J.-M. Lehn, Chem. Phys. Lett. 243 (1995) 105.
[12] S. Serroni, S. Campagna, R. Pistone-Nascone, G.S. Hanan, G.J. Davidson, J.-M. Lehn, Chem. Eur. J. 5 (1999) 3523.
[13] D. M. Bassani, J.-M. Lehn, unpublished results.
[14] B. Hasenknopf, J. Hall, J.-M. Lehn, V. Balzani, A. Credi, S. Campagna, New J. Chem. 20 (1996) 725.
[15] A. Petitjean, J.-M. Lehn, R.G. Khoury, A. DeCian, N. Kyritsakas, C. R. Chimie 5 (2002) 337.
[16] A. Petitjean, F. Puntoriero, S. Campagna, A. Juris, J.-M. Lehn, Eur. J. Inorg. Chem. (2006) 3878.
[17] (a) F.A. Cotton, Chem. Soc. Rev. 4 (1975) 27;
(b) F.A. Cotton, C.A. Murillo, R.A. Walton (Eds.), Multiple Bonds between Metal Atoms, third ed., Springer Science and Business Media, 2005.
[18] (a) P.N.W. Baxter, in: J.-M. Lehn, J.L. Atwood, J.E.D. Davies, D.D. MacNicol, F. Vögtle (Eds.), Comprehensive Supramolecular Chemistry, 9, Pergamon, Oxford, 1996, p. 254;
(b) G.S. Hanan, D. Volkmer, U.S. Schubert, J.-M. Lehn, G. Baum, D. Fenske, Angew. Chem. Int. Ed. Engl. (36) (1997) 1842.
[19] D.M. Bassani, J.-M. Lehn, S. Serroni, F. Puntoriero, S. Campagna, Chem. Eur. J. 9 (2003) 5936.
[20] (a) M. Ruben, E. Breuning, J.-P. Gisselbrecht, J.-M. Lehn, Angew. Chem. Int. Ed. 39 (2000) 4139;
(b) M. Ruben, E. Breuning, M. Barboiu, J.-P. Gisselbrecht, J.-M. Lehn, Chem. Eur. J. 9 (2003) 291.
[21] In somewhat related molecular grids based on cobalt(II) and cobalt (III) subunits, also protonic modulation of redox properties have been achieved. See: L.H. Uppadine, J.-P. Gisselbrecht, J.-M. Lehn, Chem. Commun. (2004) 718.
[22] C.S. Lent, B. Isaksen, M. Lieberman, J. Am. Chem. Soc. 125 (2003) 1056, and references therein.
[23] (a) T. Bark, M. Düggeli, H. Stoeckli-Evans, A. von Zelewsky, Angew. Chem. Int. Ed. 40 (2001) 2848;
(b) T. Bark, H. Stoeckli-Evans, A. von Zelewsky, J. Chem. Soc. Perkin Trans. I (2002) 1881.
[24] A.-M. Stadler, F. Puntoriero, S. Campagna, N. Kyritsakas, R. Welter, J.-M. Lehn, Chem. Eur. J. 11 (2005) 3997.
[25] A.-M. Stadler, F. Puntoriero, et al., unpublished results.
[26] F. Loiseau, F. Nastasi, A.-M. Stadler, S. Campagna, J.-M. Lehn, Angew. Chem. Int. Ed. 46 (2007) 6144.
[27] A. Kirsch-De Mesmaeker, L. Jacquet, A. Masschelein, F. Vanhecke, K. Heremans, Inorg. Chem. 28 (1989) 2465.
[28] M.N. Paddon-Row, in: V. Balzani (Ed.), Electron Transfer in Chemistry, vol. 3, Wiley-VCH, Weinheim, 2001, p. 179, and references therein.
[29] B. Schlicke, P. Belser, L. De Cola, E. Sabbioni, V. Balzani, J. Am. Chem. Soc. 21 (1999) 4207.
[30] S.F. Nelsen, H.Q. Tran, M.A. Nagy, J. Am. Chem. Soc. 120 (1998) 298.